Supporting Information

Strain and Hole Gas Induced Raman Shifts in Ge-Si_xGe_{1-x} Core-Shell Nanowires Using Tip-Enhanced Raman Spectroscopy

*Zhongjian Zhang[1], David C. Dillen[1], Emanuel Tutuc[1], and Edward T. Yu[1,]**

[1]Microelectronics Research Center, University of Texas, Austin, Texas, 78758, USA

*Email: ety@ece.utexas.edu

Table of Contents:

Section S1: Nanowire Structural Characterization

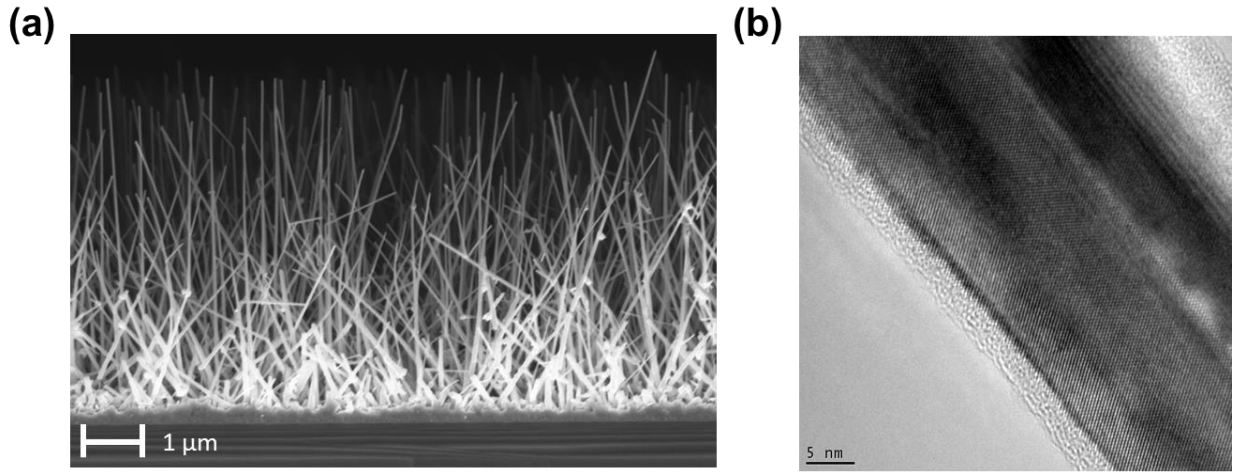

SF1. (a) A 90 degrees SEM cross sectional image of Ge-$Si_{0.5}Ge_{0.5}$ core-shell nanowire growth on Si(111) substrate. **(b)** TEM image showing lattice fringes of the core-shell nanowire

The orientation of the substrate has a minimal effect on the axial direction of the nanowires. The axial direction is primarily controlled by surface energetics and is consistently [111] for the diameter range under investigation. The nanowires do grow epitaxial to the substrate and have a predominately vertical orientation.

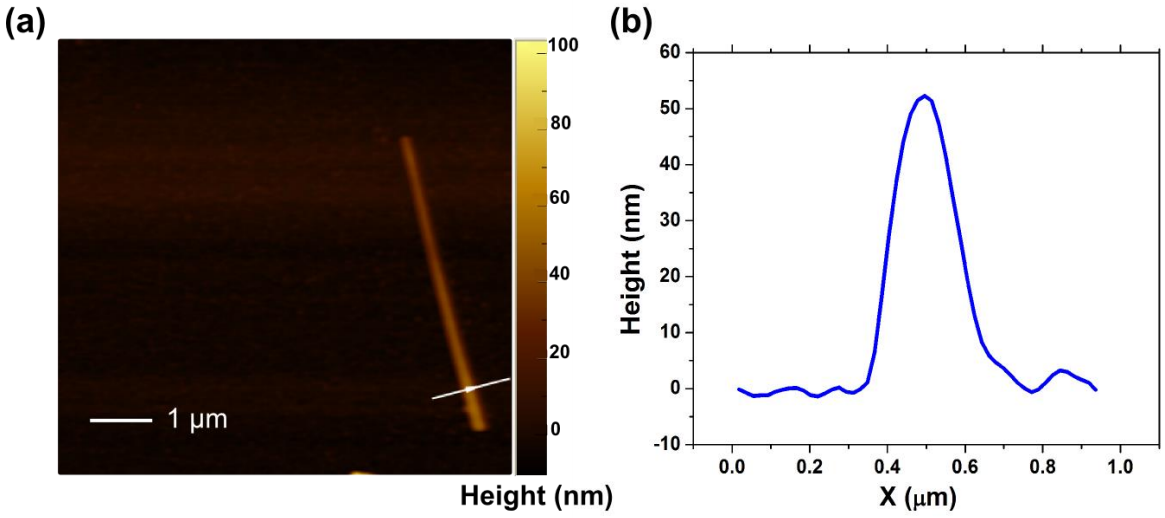

SF2. (a) Topographic AFM image of a typical Ge-$Si_{0.5}Ge_{0.5}$ core-shell nanowire dispersed on Au substrate. **(b)** Height profile of the nanowire along the line indicated by the arrowed white line in Fig. SF4a.

A typical measured nanowire is separated from other nanowires by at least a few microns.

Section S2: Nanowire Electrical Characterization, Transport Simulations, and Band Structure

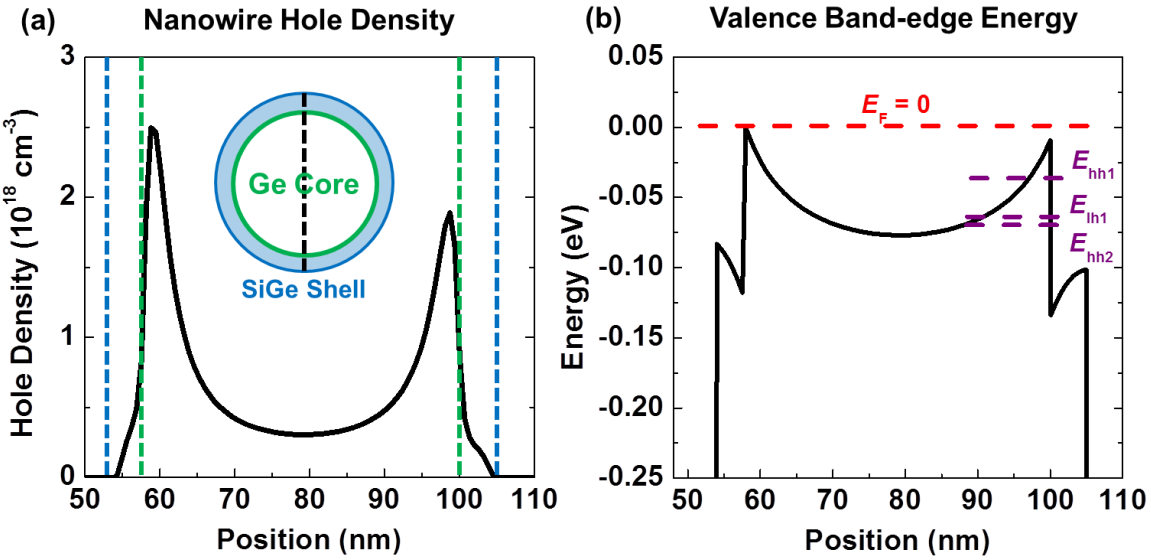

SF3. (a) Simulated hole density at zero back gate voltage with full quantum solution in a Ge-$Si_{0.5}Ge_{0.5}$ core-shell nanowire. The following parameters were used: core thickness, d = 42 nm, a shell thickness, T_{sh} = 5 nm, a core/shell valence band offset = 130 meV, and a back-gate SiO_2 thickness = 54 nm. The blue and green dashed lines indicate the border of the nanowire and the core-shell interface, respectively. The dashed black line in the inset shows the plane from which the hole density and valence band edge energy correspond with. Peak hole density in core is 2.5×10^{18} and 1.9×10^{18} cm^{-3} at the bottom and top of the NW, respectively. **(b)** Simulated band edge energy diagram for the valence band for the same core-shell nanowires. The dashed red line indicates the Fermi level. The top of the nanowire is the region closest to the tip apex and therefore of most interest. The dashed purple lines indicate confinement energies for the first and second heavy hole bands, E_{hh1} and E_{hh2}, and the first light band, E_{lh1}. The confinement energies were approximated by modeling the interface region as a triangular well. The average electric field used in the triangular well approximation is taken from the band edge energy diagram over 12nm towards the center of the Ge core from the interface.

To shift the threshold voltage to match experimental data ($V_{th} \approx 4.5$V), 2×10^{18} cm^{-3} boron doping was added to shell. The core remains undoped. Band offsets used for the simulation were taken from previous results.[1] The electric field approximation for the triangular well underestimates the electric field closer to the interface; however, this is offset by the overestimation of the barrier height, which is assumed to be of infinite height, in the triangular well approximation when in actuality the barrier is significantly smaller.

For bulk Ge, the heavy hole effective mass is $0.33m_e$, and the light hole effective mass is $0.043m_e$. For the 2D hole gas in the interface region of the core shell nanowire, the heavy hole transvers effective mass is $0.0568m_e$, and the light hole transverse effective mass is $0.1099m_e$.

When comparing the two valence band curvatures, the heavy hole band in the nanowire case has significantly more curvature than the heavy hole band in the bulk case, and the light hole bands have comparable curvature in both cases The much greater curvature would indicate a higher number of occupied and unoccupied states for carrier transitions to occur. Based on a carrier concentration of 2×10^{18} cm^{-3}, the sheet density for the 2DHG at the nanowire interface would be 1.59×10^{12} cm^{-2}, which would only fill the first heavy hole subband of the valence band. The Fermi level is then below the top of the valence band, which allows intervalence-band transitions to occur between the subbands.[2]

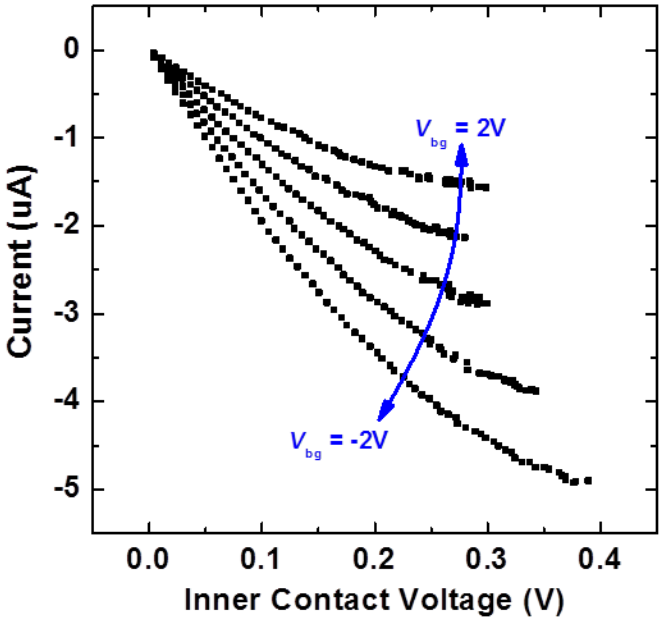

SF4. Four point electrical measurements used to determine nanowire carrier density.

As stated in the main text, electrical measurements were performed on a back-gated four-point device with 54 nm SiO2 dielectric and boron implanted regions under Ni contacts with a device channel length of 1100nm, Ge core diameter of 42nm, and Si0.5Ge0.5 shell thickness of 5nm.

Section S3: Strain Calculations

The calculated Raman shift due to strain was determined by solving the secular equation obtained from lattice dynamical theory:[3]

$$\begin{pmatrix} p\varepsilon'_{11} + q(\varepsilon'_{22} + \varepsilon'_{33}) - \lambda_1 & 2r\varepsilon'_{12} & 2r\varepsilon'_{13} \\ 2r\varepsilon'_{12} & p\varepsilon'_{22} + q(\varepsilon'_{11} + \varepsilon'_{33}) - \lambda_2 & 2r\varepsilon'_{23} \\ 2r\varepsilon'_{13} & 2r\varepsilon'_{23} & p\varepsilon'_{33} + q(\varepsilon'_{11} + \varepsilon'_{22}) - \lambda_3 \end{pmatrix} = 0 \qquad (1)$$

The term *p*, *q*, and *r* are the Ge core phonon deformation potential values, ε_{ii} indicates the values of the strain tensor, and λ_i are the wavelengths of the Raman modes. Eq. (1) can be simplified by taking into account the form of the strain tensor in the core due to the cylindrical symmetry of the NW. By taking the z-axis to be in the direction of the NW main axis, the [111] direction and the x and y axes as the $[1\bar{1}0]$ and $[11\bar{2}]$ directions, respectively, the strain tensor is then of the form:[4,5]

$$\boldsymbol{\varepsilon} = \begin{pmatrix} \varepsilon_{rr} & 0 & 0 \\ 0 & \varepsilon_{rr} & 0 \\ 0 & 0 & \varepsilon_{zz} \end{pmatrix}, \qquad (2)$$

where the in-plane components ε_{xx} and ε_{yy} are equal and labeled as ε_{rr}. The off-diagonal shear components The strain tensor is then converted into a crystal-oriented coordinate system where the x', y', and z' axes correspond to the [100], [010], and [001] directions, respectively. Using the following tensor transformation:

$$\varepsilon'_{ij} = \sum_{pq} a_{ip} a_{jq} \varepsilon_{pq}, \qquad (3)$$

where

$$\mathbf{a} = \begin{pmatrix} 1/\sqrt{2} & 1/\sqrt{6} & 1/\sqrt{3} \\ -1/\sqrt{2} & 1/\sqrt{6} & 1/\sqrt{3} \\ 0 & -2/\sqrt{6} & 1/\sqrt{3} \end{pmatrix}, \qquad (4)$$

This results in the following strain tensor:

$$\boldsymbol{\varepsilon}' = \begin{pmatrix} \frac{2}{3}\varepsilon_{rr} + \frac{1}{3}\varepsilon_{zz} & \frac{-1}{3}\varepsilon_{rr} + \frac{1}{3}\varepsilon_{zz} & \frac{-1}{3}\varepsilon_{rr} + \frac{1}{3}\varepsilon_{zz} \\ \frac{-1}{3}\varepsilon_{rr} + \frac{1}{3}\varepsilon_{zz} & \frac{2}{3}\varepsilon_{rr} + \frac{1}{3}\varepsilon_{zz} & \frac{-1}{3}\varepsilon_{rr} + \frac{1}{3}\varepsilon_{zz} \\ \frac{-1}{3}\varepsilon_{rr} + \frac{1}{3}\varepsilon_{zz} & \frac{-1}{3}\varepsilon_{rr} + \frac{1}{3}\varepsilon_{zz} & \frac{2}{3}\varepsilon_{rr} + \frac{1}{3}\varepsilon_{zz} \end{pmatrix}, \quad (5)$$

By substituting Eq. (5) into Eq. (1), a nondegenerate singlet mode $\lambda_s = \lambda_1$ and a degenerate doublet mode $\lambda_d = \lambda_2 = \lambda_3$ are obtained:

$$\lambda_1 = \varepsilon_{zz}\left[\frac{1}{3}p + \frac{2}{3}q + \frac{4}{3}r\right] + \varepsilon_{rr}\left[\frac{2}{3}p + \frac{4}{3}q - \frac{4}{3}r\right],$$

$$\lambda_{2,3} = \varepsilon_{zz}\left[\frac{1}{3}p + \frac{2}{3}q - \frac{2}{3}r\right] + \varepsilon_{rr}\left[\frac{2}{3}p + \frac{4}{3}q + \frac{2}{3}r\right], \quad (6)$$

Using the polarization selection rule:[6]

$$I_i \propto \left|\vec{E}_{inc}^{T} \cdot \boldsymbol{R'}_i \cdot \vec{E}_{scat}\right|^2, \quad (7)$$

where

$$\boldsymbol{R'}_i = \sum_j \left(\vec{u}_j \cdot \vec{u}'_i\right) \boldsymbol{R}_j, \quad (8)$$

the relative intensities I_i, can be determined for the three Ge-Ge modes λ_i from Eq. (6). The unstrained phonon wavevectors, $\vec{u}_j$, are given by $\vec{u}_1 = [100]$, $\vec{u}_2 = [010]$, and $\vec{u}_3 = [001]$. $\vec{u}'_i$ are the phonon wavevectors under strain, where the values were found through a solution of Eq. (1) using a strain tensor of the form of Eq. (2) with arbitrary values for ε_{rr} and ε_{zz}. $\vec{E}_{inc}^{T}$ and $\vec{E}_{scat}$ are the polarization vectors of the incident and scattered light, respectively. $\boldsymbol{R'}_i$ are the Raman tensors of the perturbed system, while $\boldsymbol{R}_j$ are those of the unstrained cubic system.[7] After calculating the Raman intensities of the three Ge-Ge modes, it was determined that the singlet mode had the highest relative intensity and was the one being observed. The following constants were then used to determine the theoretical Raman shift:

p/w_0^2	q/w_0^2	r/w_0^2	a_{core} (Å)	a_{shell} (Å)	$E_{[111]}$ (GPa)	v	t (N/m)
-1.66[8]	-2.19[8]	-1.11[9]	5.658[10]	5.538[10]	155[10]	0.16[10]	1.00[5]

Section S4: Electromagnetic Simulations

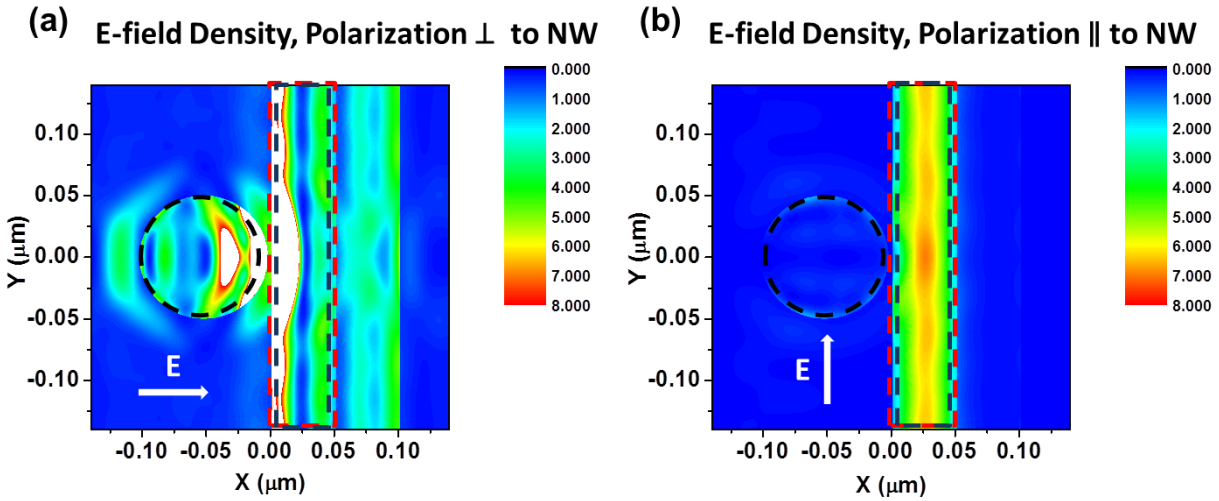

SF5. Computational electromagnetic simulations. Shown are results along the center of the nanowire in the x-y plane of the electric field density for **(a)** an electric field polarization of 30° in relation to the x-axis and **(b)** an electric field polarization along the y-axis. Both simulations are performed with the tip within 3 nm of the nanowire.

S3 shows that when the electric field is polarized along the direction of the nanowire axis, the electric field density within the wire is significantly higher than when it is perpendicular to the nanowire axis. In the x-polarization case, the polarization is the same as in Figure 4.

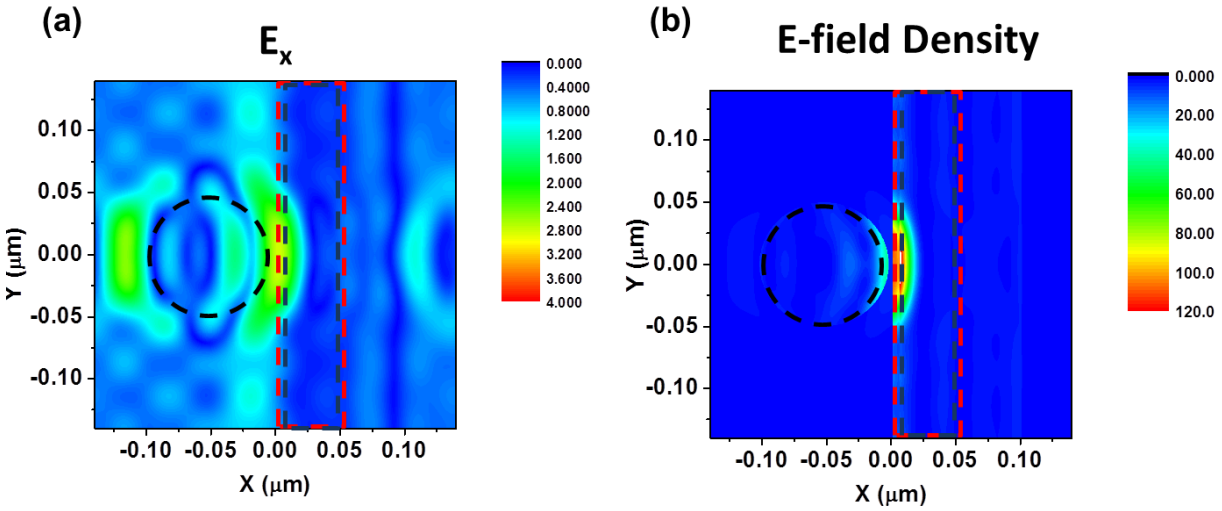

SF6. Computational electromagnetic simulations. Spatial cuts along the center of the nanowire in the x-y plane of **(a)** E_x and **(b)** the electric field density are shown. Both simulations are performed with the tip within 3 nm of the nanowire.

The features in the spatial field distribution at the interface region are very similar for both the electric field component in the x-direction (E_x) and the electric field density plots. The electric

field density is defined by: $U_E(\boldsymbol{r}') = \frac{1}{2} Re[\varepsilon(\boldsymbol{r}')]|\boldsymbol{E}(\boldsymbol{r}')|^2$. The qualitative similarity between the two plots indicates that E_x is the dominant component in the electric field density, which is why E_x is used to calculate the 2D FFTs.

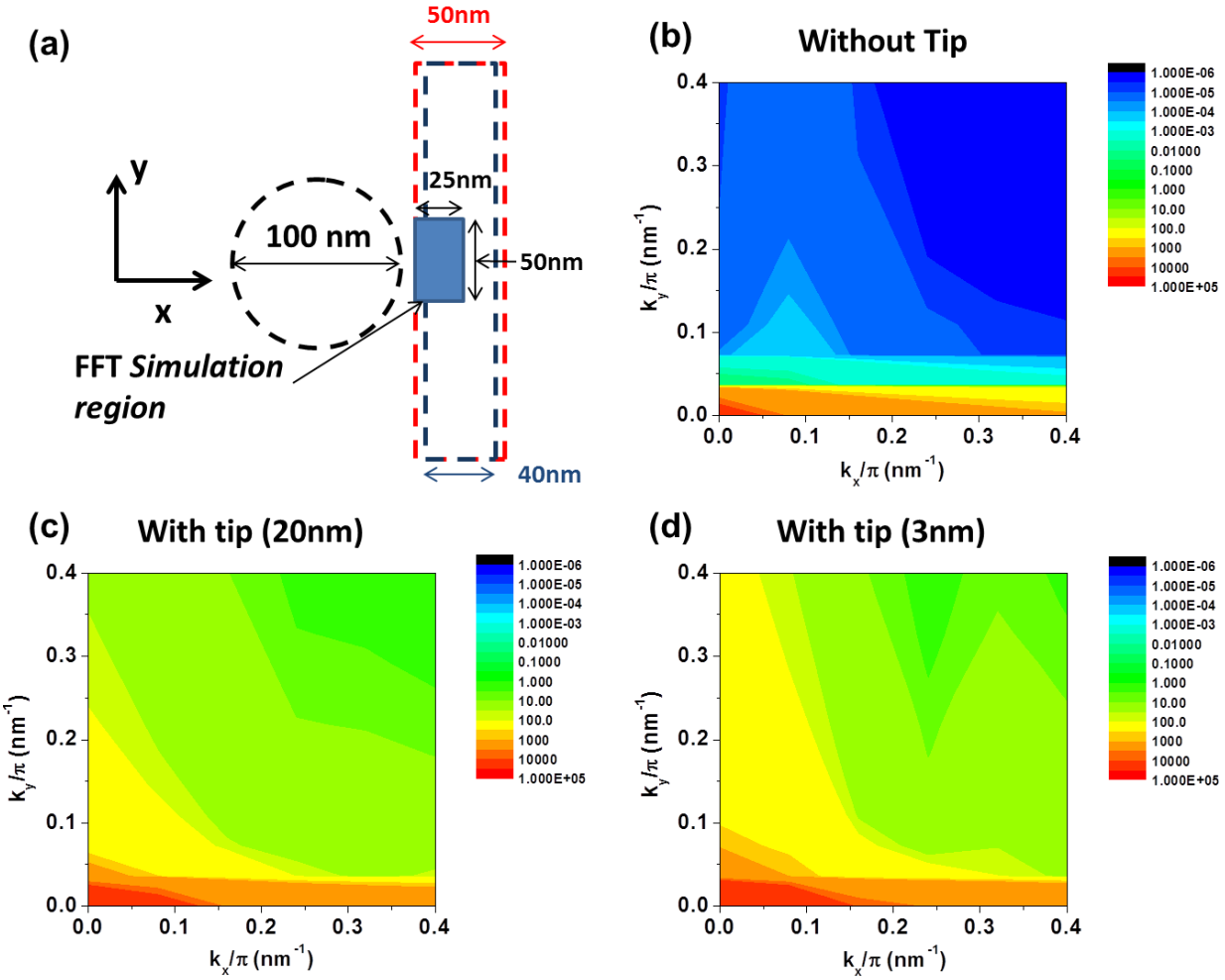

SF7. 2D FFT computations from our spatial electric field simulation data **(a)** Shows the simulation region used to compute the 2D FFTs. Computation results for the cases **(b)** with no tip, **(c)** with a tip 20 nm from the nanowire, and **(d)** with a tip 3 nm from the nanowire.

2D Fast Fourier transforms were performed on spatial electric field computation simulations for E_x. In the case without the tip, the Fourier amplitudes are significantly for all wavevector values, when compared to the two cases with the tip. When comparing the 20 nm and 3 nm cases, the 3 nm case has higher Fourier amplitudes at all wavevector values.

Section S5: Raman Shift Analysis

For heavily p-type Si and Ge, the dominant mechanism that causes the significant red shift in the Raman spectra when compared to the intrinsic material is intervalence band carrier transitions rather than intravalence band carrier transitions, although both types of transitions may occur.[11] The Raman shift caused by the intervalence band transitions can be described by[12]

$$\hbar\Gamma(\omega) = \pi \int \rho(\hbar\omega)\langle|\langle\psi_i|H|\phi\rangle|^2\rangle_{av}\, dV, \tag{9}$$

where Γ is the magnitude of the Raman shift, $\rho(\hbar\omega)$ is the combined density of states for the continuum of intervalence band transitions, $\langle|\langle\psi_i|H|\phi\rangle|^2\rangle_{av}$ is the average matrix element of the electron-phonon interaction for different symmetry directions, and the integral is computed over the nanowire crystal volume. By assuming the average matrix element is independent of energy and by computing the two-band electron-phonon matrix element using the deformation potential approximation for 26 directions in *k* space (6{100}, 8{111}, and 12 {110}), this leads to a value given by[12]

$$\langle|\langle\psi_i|H|\phi\rangle|^2\rangle_{av} = \frac{95}{78}\left(\frac{1}{2}\delta E\right)^2, \tag{10}$$

where $\delta E$is the splitting of the top of the valence band produced by the k = 0 optical phonon. Assuming δE is constant for the excitation volume of the crystal, the splitting for the ground state zero-point phonon is given by[12]

$$\delta E = \left(\frac{a^3\hbar}{4MV_{ex}\Omega}\right)^{1/2}\frac{2d_0}{a}(1+n_B)^{1/2}, \tag{11}$$

where *a* is the lattice constant, *M* is the ionic mass, V_{ex} is the excitation crystal volume, d_0 is the deformation potential and n_B is the number of phonons which are distributed in energy according to the Bose-Einstein distribution, which relates directly to the number of phonons involved in the splitting of the top of the valence band. By assuming both $\rho(\hbar\omega)$ is also constant for the excitation volume, the expression for Γ is then[12]

$$\hbar\Gamma = \frac{\pi}{4}\left(\frac{95}{78}\right)\frac{\hbar a}{M\Omega}d_0^2\rho(\hbar\omega)(1+n_B). \tag{12}$$

To evaluate Γ, a numerical estimate of ρ must be obtained, which can be determined by its value at the Fermi energy (μ), by assuming limited variation in $\rho(\hbar\omega)$ in the neighborhood of $\omega = \Omega$. Parabolic bands can be assumed with masses m_h and m_l for the heavy hole and light hole valence bands. Using these assumptions, the density of states is given by[12]

$$\rho(\mu) \cong \frac{3}{2}\frac{\alpha^{3/2}}{(1-\alpha)^{3/2}(1-\alpha^{3/2})}\frac{N_h - N_l}{\mu}, \tag{13}$$

where $= m_l/m_h = 0.22$, for heavy hole and light hole effective masses for Ge calculated using the k.p method.

In the case of the interface region of the nanowire in close proximity to the probe tip, additional wavevector values are produced by the changed spatial field distribution. Additional wavevector values relax momentum conservation constraints and results in a greater number of

phonons involved in the intervalence band transitions. This now means that instead of just taking into account the effect of the k = 0 optical phonon, a distribution of phonons, with the maximum centered at k = 0, contribute to the intervalence band carrier transitions. An increase in intervalence band carrier transitions would result in a pronounced increase in the red shift of the Raman spectrum. To quantify this increased change, the value of n_B must be first determined. The value of Γ can be compared to the Raman shifts measured in the case without the tip to determine the appropriate value of n_B that will be used in further calculations. For a Raman shift of ~1.2 cm^{-1}, which is the average for our Raman measurements without the tip, we obtain a value for n_B of 0.62. To incorporate the effect of the tip, an additional distribution function representing the distribution of additional phonons allowed by momentum conservation relaxation is convoluted with Eq. (12) to represent the distribution of phonons that are now allowed instead of just the zone center optical phonon.[13] This yields an equation for the Raman shift given by

$$\hbar\Gamma = \frac{\pi}{4}\left(\frac{95}{78}\right)\frac{\hbar a}{M\Omega} d_0^2(1+n_B)\int \rho(\hbar\omega')h(\hbar\omega')d\omega', \qquad (14)$$

where $h(\hbar\omega)$ is the distribution function for the allowed phonons. Because $\rho(\hbar\omega)$is very flat around $\omega = \Omega$, the value can be taken as a constant with a value determined by Eq. (13). Solving the integral for Eq. (14) is now simple and yields:

$$\hbar\Gamma = \frac{\pi}{4}\left(\frac{95}{78}\right)\frac{\hbar a}{M\Omega} d_0^2(1+n_B)\,\rho(\mu)h_d, \qquad (15)$$

where h_d is the value of the integral of the phonon distribution function. For a Γ of 4.2 and 8.4 cm^{-1}, the lower and upper bounds for the interface peak Raman shift for 3 nm tapping amplitude measurements, the values for h_d are 3.5 and 7.0, respectively. The average Γ for conventional Raman measurements is 1.0, which corresponds to a h_d of 0.83. If the conventional Raman results are used to normalize the distribution function, the resulting full width half maximum (FWHM) of h_d for the lower bound and upper bound for 3 nm tapping amplitude measurements would be 2.4 cm^{-1} and 4.7 cm^{-1}. In previous results relating optical phonons and acceptor continuum states in Si, the FWHM for the phonon distribution was found to be ~15 cm^{-1} which is greater but still reasonably close to the values determined in the TERS measurement.[13]

Section S6: Additional Figures

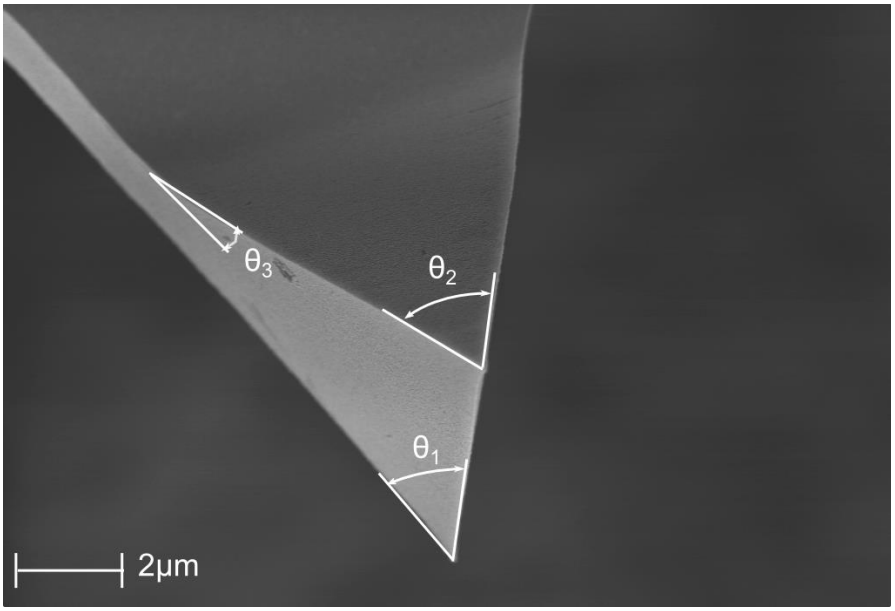

SF8. SEM image of typical Au coated AFM tip used for TERS measurements.

The image shows a lower magnification image of the tip. The front angle θ_1, side angle θ_2, and back angle θ_3 are 90°, 70°, and 35°, respectively. These angles come from supplier specifications.

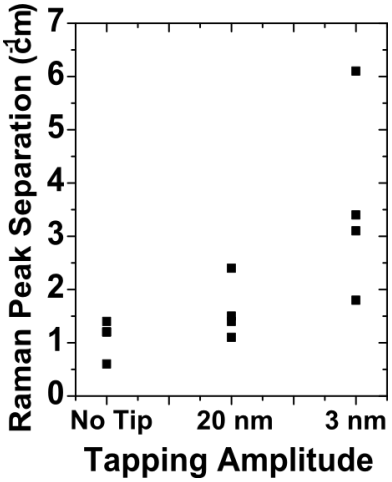

SF9. The separation between the core and interface peaks for our three measurement conditions with vertically polarized laser excitation.

Measurements with a vertical polarizer along the excitation laser path show the same trend as with previous measurements without the polarizer. Difference in the precise values of Raman peak separation as a function of tip tapping amplitude occur due to variations in tip shape and size at the nanoscale, as also seen in Fig. 5c (in the main text).

References

1. Nah, J., Dillen, D. C., Varahramyan, K. M., Banerjee, S. K. & Tutuc, E. Role of confinement on carrier transport in Ge-Si(x)Ge(1-x) core-shell nanowires. *Nano Lett.* **12,** 108–12 (2012).

2. Olego, D., Cardona, M. & Rössler, U. Intra- and inter-valence-band electronic Raman scattering in heavily doped p-GaAs. *Phys. Rev. B* **22,** 1905–1911 (1980).

3. Ganesan, S., Maradudin, A. . & Oitmaa, J. A lattice theory of morphic effects in crystals of the diamond structure. *Ann. Phys. (N. Y).* **56,** 556–594 (1970).

4. Liang, Y., Nix, W. D., Griffin, P. B. & Plummer, J. D. Critical thickness enhancement of epitaxial SiGe films grown on small structures. *J. Appl. Phys.* **97,** 043519 (2005).

5. Schmidt, V., McIntyre, P. & Gösele, U. Morphological instability of misfit-strained core-shell nanowires. *Phys. Rev. B* **77,** 235302 (2008).

6. Menéndez, J., Singh, R. & Drucker, J. Theory of strain effects on the Raman spectrum of Si-Ge core-shell nanowires. *Ann. Phys.* **523,** 145–156 (2011).

7. Loudon, R. The Raman effect in crystals. *Adv. Phys.* **13,** 423–482 (1964).

8. Reparaz, J. S., Bernardi, a., Goñi, a. R., Alonso, M. I. & Garriga, M. Composition dependence of the phonon strain shift coefficients of SiGe alloys revisited. *Appl. Phys. Lett.* **92,** 081909 (2008).

9. Cerdeira, F., Buchenauer, C. J., Pollak, F. H. & Cardona, M. Stress-Induced Shifts of First-Order Raman Frequencies of Diamond- and Zinc-Blende-Type Semiconductors. *Phys. Rev. B* **5,** 580–593 (1972).

10. Wortman, J. J. & Evans, R. a. Young's Modulus, Shear Modulus, and Poisson's Ratio in Silicon and Germanium. *J. Appl. Phys.* **36,** 153 (1965).

11. Olego, D. & Cardona, M. Self-energy effects of the optical phonons of heavily doped p-GaAs and p-Ge. *Phys. Rev. B* **23,** (1981).

12. Cerdeira, F., Fjeldly, T. A. & Cardona, M. Effect of Free Carriers on Zone-Center Vibrational Modes in Heavily Doped p-type Si. II. Optical Modes. *Phys. Rev. B* **8,** 4734–4745 (1973).

13. Watkins, G. & Fowler, W. Resonant interactions of optical phonons with acceptor continuum states in silicon. *Phys. Rev. B* **16,** 4524–4529 (1977).